A New Control Scheme for Three-Phase Non-Isolated Grid Feeding PV Inverter

Sumaya Jahan
Electronics & Telecommunication Engineering
Rajshahi University of Engineering & Technology
Rajshahi-6204, Bangladesh
sumaya.jahan.s15@gmail.com

Shuvra Prokash Biswas
Electronics & Telecommunication Engineering
Rajshahi University of Engineering & Technology
Rajshahi-6204, Bangladesh
spbiswas@ete.ruet.ac.bd

Md Kamal Hosain
Electronics & Telecommunication Engineering
Rajshahi University of Engineering & Technology
Rajshahi-6204, Bangladesh
khosain@ete.ruet.ac.bd

Md Rabiul Islam
School of Electrical, Computer and Telecommunications Engineering
University of Wollongong
New South Wales 2522, Australia
mrislam@uow.edu.au

Md Moktadir Rahman
Energy & Grid Divison
Ingeteam Australia Pty Ltd
New South Wales 2522, Australia
moktadir.rahman@ingeteam.com

Youguang Guo
School of Electrical and Data Engineering
University of Technology Sydney
New South Wales 2007, Australia
youguang.guo-1@uts.edu.au

***Abstract*—The use of control algorithms in inverter topologies is becoming more attractive for integration of wind and photovoltaic (PV) energy with a grid. Among the various inverters, the non-isolated inverter topology has gotten a huge attention for fixing the problem of leakage current issue with other inverters. In this paper, a linear control strategy is offered for the grid connected non-isolated PV inverter. The proposed scheme consists of a proportional resonance (PR) controller with lag compensator (LC). This controller offers lower oscillation in output grid current and better steady state performance for the grid-tied PV inverter systems. The analytical comparison of proposed control scheme and the other control strategies are mentioned in this work. The simulation results indicate the improvements of the performance for the proposed controller in terms of reference tracking ability, total harmonic distortion (THD), and the supplied dc bus voltages of the grid-injected PV inverter systems. This proposed controller can enhance the performance of the PV systems by reducing energy consumption during load change and faulty condition.**

Keywords—photovoltaic energy, three phase inverter, linear control strategy, proportional resonance controller, lag compensator, total harmonic distortion.

I. INTRODUCTION

Due to the widespread usage of renewable energy sources (RESs) in grid-connected systems, large-scale wind, tidal, and solar photovoltaic (PV) power plants have been rapidly expanding. Among all the RESs, solar PV power plants are becoming popular around the world because of the potentiality of trouble-free maintenance, smooth control, and high efficiency. In recent years, the expenditure and generating costs of grid-connected photovoltaic (PV) systems have steadily fallen. In order to reach the goals of low cost, light weight, and compact size, the PV inverters must be meticulously developed. PV energy sources also have the potential to mitigate major global issues like global warming [1]–[3].

Power electronic converters provide an advisory capacity to link the PV power plants to the grid and offer the conditioning function of the energy conversion efficiency. Two-level power converters are conventionally used for the solar power conversion system which requires a bulky size line filter to mitigate the harmonics of output voltage and current. These also require a high frequency transformer for the purpose of isolation and stepping up the voltage which results in increase of the total loss and volume of the PV systems [4]. Recently several advanced power electronic converter topologies have been presented in various works to conjugate the PV power plants to the grid. For instance, active neutral point clamped (ANPC) multilevel inverter topology [5] and three-phase non-isolated inverter [6] with the reduced number of switches have presented for enhancing the performance of the grid connected system. Non-isolated inverter provides reduced total harmonic distortion (THD), lower stress in voltages, lesser losses for the filter components, and smaller leakage current.

The inverter control design is extremely essential for developing grid-connected PV power system. Different control algorithms have been applied in several works in literature to increase the performance of the system regarding the stability factor, responses of grid outlets and THD profile [7]–[11]. For example, in [7], the performance of several conventional and advanced control methods were studied for multi-level inverter (MLI) fed grid linked PV systems. High-performance control approaches as well as objections to such techniques were mentioned and emphasized in this paper. The hybrid modulation technique and a double-loop current control method constructed in a hybrid reference frame were both investigated in [8]. These methods were applied in MLI topology to improve the weak grid condition of the system. Conventional proportional integral (PI) control strategy was utilized for the double-loop current control method which offered a satisfactory profile in dynamic response and steady state performance of the system. However, the MLI inverter increased the number of switch count in the system. Moreover, an advanced control method was analyzed in [9] which was the combination of PI controller and lead-lag compensator (LLC). It provided lower THD and ensured almost zero phase shift of the output voltage and current in a neutral point clamped (NPC) inverter fed grid-tied PV systems. This system faced troubles with the capacitor voltage balancing issue of the NPC inverter. In another study, proportional resonance (PR) controller was analyzed with the harmonic compensator (HC) techniques in [10] for the direct

current control in a grid connected inverter system. Zero compensation term was introduced to increase the stability and suppress the distortion of output grid current and voltage. However, the grid conditions under some disturbances were not mentioned in this paper. Furthermore, a proportional integral resonance (PIR) current control technique was demonstrated in [11] to control 15-level NPC inverter for the grid connected PV application. It showed admirable performance to handling the performance of inverter and grid outlets under the changed load and fault condition of the system.

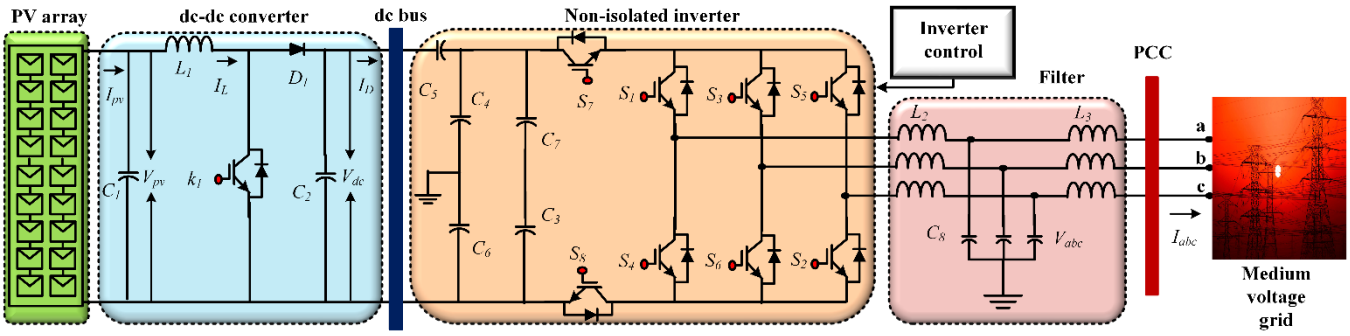

Fig 1. Block diagram of the grid-connected non-isolated PV inverter system.

In this work, a new control scheme is proposed to enhance the performance of the grid connected PV inverter system. This control scheme consists of PR controller with the feedback of lag compensator (LC). This lag compensator improves the steady state response of the system. The proposed control technique is designed to control the non-isolated inverter topology [5] for its superior performance in the PV system. This control technique minimizes the shortcomings of other control strategies mentioned in the literature.

This paper is organized as follows: system specification and description are included in section II. The conventional control strategies are shown in section III. The proposed control scheme in included section IV. The performance analysis of the proposed control strategy done in section V and finally section VI concludes this paper.

II. System Specification and Description

The block diagram of the non-isolated inverter fed grid-connected PV systems is shown in Fig. 1. Here, PV array supplies the total power to operate this system. PV array supplies output PV voltage and current which is then utilized to supply the input power of the inverter. The output PV voltage is not directly acceptable for the inverter input because of its oscillatory nature. Thus, this voltage is fed to the dc to dc inverter of the PV system. The dc to dc inverter converts the output PV voltage in a uniform dc voltage source for the inverter. The dc-dc inverter utilizes the output PV current and voltage through maximum power point tracking algorithm to generate the required duty cycle of this converter. This duty cycle helps to generate the switching pulse and to operate the dc to dc converter. This converter results the output dc voltage which is then supplied to the dc to ac converter named as non-isolated inverter. The output dc voltage can be expressed as [12]:

$$V_{dc} = \frac{(1-k_1)I_L - I_D}{C_2} \quad (1)$$

Here, k_1 represents the duty cycle, I_L and I_D represent the inductor current and the output current of dc to dc converter respectively. C_2 defines the dc-link capacitor and V_{dc} represents the dc-link voltage of the inverter. In this system, a grid-tied two-level three-phase non-isolated inverter is used for applying the proposed control method. This inverter consists of eight insulated-gate bipolar transistor (IGBT) switches among them S_7 and S_8 are dedicated for isolating the dc stages. Inverter output voltage and current are obtained by operating this switching devices of the inverter. Here, an LCL filter is used to suppress the harmonic of the inverter voltage and current. The grid is connected to the inverter through this filter. The performance of the output grid outlets can be observed at the point of common coupling (PCC) of the system. Inverter control is used to control the inverter voltage and current and to achieve desired grid output voltage and current.

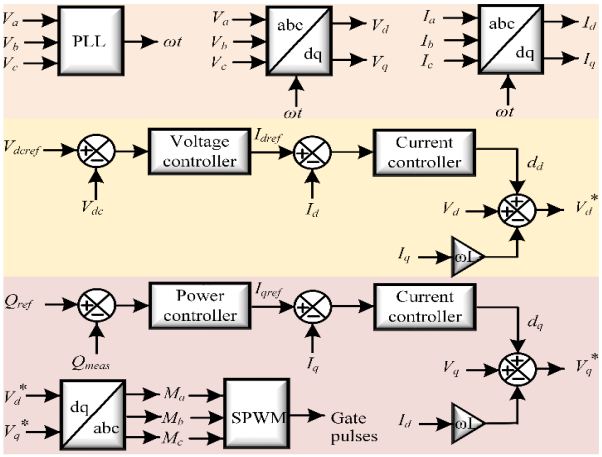

Fig. 2. Block diagram of the inverter control unit.

The detailed block diagram of inverter control unit is demonstrated in Fig. 2. Here, the voltage and current are transformed from abc domain to dq domain. A phase locked loop (PLL) is used for synchronization of the grid which offers a phase angle (ωt) for the transformation. This control technique works as outer loop controller and inner loop controller. Outer loop controllers are used to determine the reference currents for the inner loop current control strategy. Reference dc-link voltage (V_{dcref}) and the measured dc-link voltage (V_{dc}) are used by the voltage controller to produce the reference direct axis current component (I_{dref}). Reference quadrature axis current component (I_{qref}) is obtained by utilizing the error of the reference reactive power (Q_{ref}) and

measured reactive power (Q_{meas}). Then the reference current components are compared with the measured direct axis current (I_d) and quadrature axis current component (I_q) to calculate the error. These errors are then used by the anticipated current control strategy to produce the gate pulses of the non-isolated inverter. The output of the controller is transformed from the dq domain to the abc domain to determine the desired modulating signal. This modulating signal is then compared with a high frequency carrier signal to attain the gate pulses for the IGBT switches of the inverter by the sinusoidal pulse width modulation (SPWM) technique.

III. Conventional Control Techniques

For improving the quality of output power and the efficiency of the inverter, the control technique has drawn the most significant attention in the inverter-based PV systems because of its ease implementation. Proportional integral (PI) control technique is the most popular control technique because of its simplicity in operation. Other linear control techniques including proportional integral derivative (PID), proportional resonance (PR) and proportional integral resonance (PIR) control techniques are designed based on the PI controller. The transfer functions of the corresponding control strategies are expressed as:

$$T_{PI}(s) = k_p + \frac{k_i}{s} \tag{2}$$

$$T_{PID}(s) = k_p + \frac{k_i}{s} + k_d s \tag{3}$$

$$T_{PR}(s) = k_p + \frac{k_r s}{s^2 + \omega_r^2} \tag{4}$$

$$T_{PIR}(s) = k_p + \frac{k_i}{s} + \frac{k_r s}{s^2 + \omega_r^2} \tag{5}$$

where, k_p, k_i, and k_r are different constant of these control techniques named as proportional constant, integral constant, and resonance constant respectively.

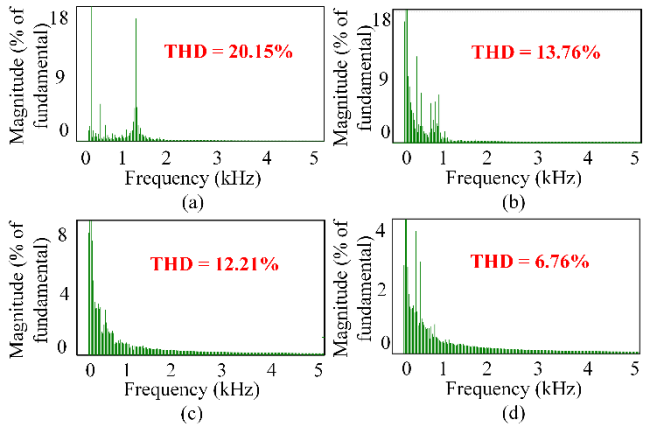

Fig. 3. Frequency spectra of output current waveforms of the three-phase non-isolated inverter with the various control techniques: (a) PI controller, (b) PID controller, (c) PR controller and (d) PIR controller.

These constant causes a considerable impact in the performance of these control schemes. The frequency spectra of output grid current of three-phase non-isolated inverter with the conventional control strategies are displayed in Fig. 3. Considering the THD profile of the of the conventional control techniques mentioned in the frequency spectra, PI controller offers very high THD of 20.15% and shows very poorest performance among all the controllers. Among other control techniques 13.76% THD is offered for PID controller, 12.21% THD for PR controller and 6.76% THD for the PIR controller. PIR controller offers the lowest THD and better performance than the other controllers. These conventional control schemes show substantial amount of THD in the output current waveforms which decrease the efficiency of the system and affect the power quality of the inverter. This also affects the output current waveforms by introducing the oscillation.

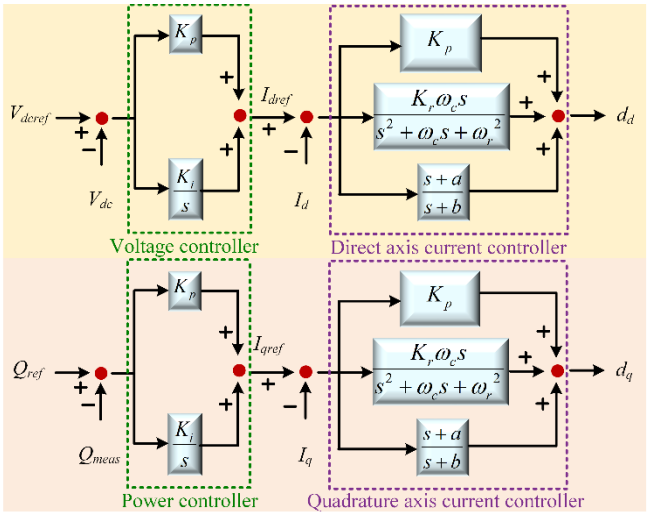

Fig. 4. Block diagram of the proposed control scheme.

IV. Proposed Control Technique

The block diagram of the proposed control scheme is depicted in Fig. 4. It represents two control loops. One is outer control loop and another is inner control loop. The outer control loops denote the voltage controller and the power controller. On the contrary, the inner control loops are the current controllers for the direct axis and the quadrature axis. Outer loop controllers are the conventional PI controller and the inner loop controllers are the proposed controller. This proposed control technique is basically a PR controller with the feedback of lag compensator (LC) and it is named as PR+LC controller. The transfer function of the proposed control technique can be denoted as:

$$T_p(s) = K_p \tag{6}$$

$$T_R(s) = \frac{K_r \omega_c s}{s^2 + \omega_c s + \omega_r^2} \tag{7}$$

$$T_{LC}(s) = \frac{s+a}{s+b} \tag{8}$$

$$T(s) = T_P(s) + T_R(s) + T_{LC}(s) \tag{9}$$

$$T(s) = K_p + \frac{K_r \omega_c s}{s^2 + \omega_c s + \omega_r^2} + \frac{s+a}{s+b} \tag{10}$$

where K_p, K_i, and Kr are proportional, integral and resonant constants. a and b are the compensator constant with a > b. These constants can be varied to achieve the better performance of the offered control scheme.

Fig. 5 shows the bode diagram of outer loop voltage and inner loop current controllers. The bandwidth of proposed PR+LC controller is greater than the bandwidth of the conventional PI controller. Higher bandwidth results better transient response of the controller. Moreover, higher phase value increases the stability of the system. This proposed PR+LC controller offers the magnitude of 222 dB and the phage of 88.7 degree. The outer loop controller bandwidth is much lower than the current controller.

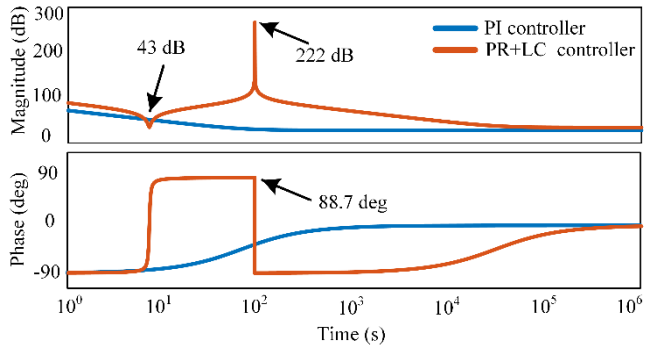

Fig. 5. The bode diagram of the outer loop and inner loop controller.

V. Performance Analysis of the Non-Isolated Inverter Based PV Systems

The performance of the non-isolated inverter fed grid-tied PV system is observed through the simulation process in MATLAB/Simulink environment. The performance of output voltage and current response, power response, dc-link voltage waveform, load change response of the inverter, and the steady state response are observed to validate the superiority of the prosed controller in the grid-tied PV inverter system.

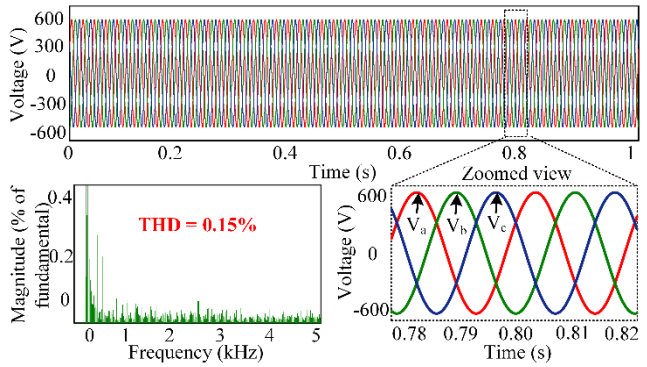

Fig. 6. The response of output grid voltage and its frequency spectrum.

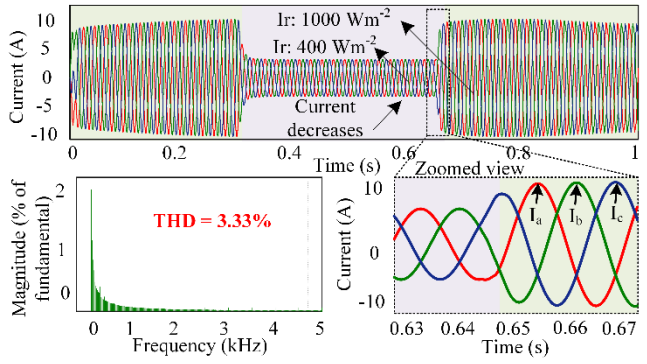

Fig. 7. The response of output grid current and its frequency spectrum.

Fig. 6 and Fig. 7 display the output grid voltage and current waveforms of the system. These output waveforms are observed by varying the irradiance condition of the PV array. There is no effect of that variation in the voltage waveform which is shown in Fig. 6. Its frequency response denotes 0.15% THD of the grid voltage. Irradiance variation causes the change in output response of grid current mentioned in Fig. 7. A 3.33% THD of output grid current is displayed in the frequency spectrum of Fig.7.

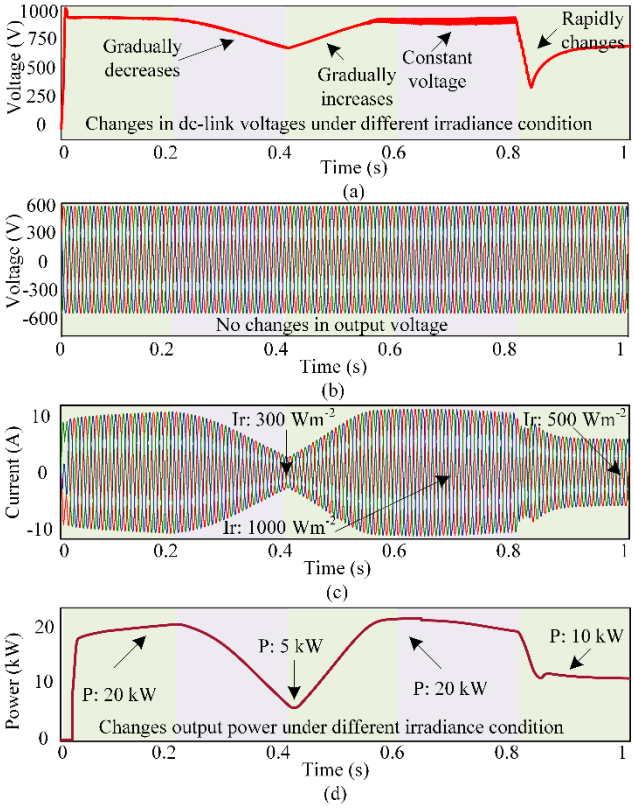

Fig. 8. The response of the grid-tied PV system by varying the irradiance of the PV array: (a) dc-link voltage, (b) output grid voltage, (c) output grid current, and (d) output power.

By varying the irradiance of the system in different time period, the system performances parameters including the dc-link voltage, output current waveform, output voltage waveform, and the output power are observed. In time 0 to 0.2s, the irradiance is set to 1000 Wm^{-2}, then it gradually decreases from 1000 to 300 Wm^{-2} in time duration of 0.2s to 0.4s, the irradiance gradually increases from 300 to 1000 Wm^{-2} in time 0.4s to 0.6s, it remains constant at 1000Wm^{-2} in time period of 0.6s to 0.8s and finally a sudden rapid variation of 1000 to 500 Wm^{-2} is occurred in time 0.8s to 1s. The proposed system shows very good performance by responding against this variation. The dc-link voltage firstly remains constant at 800 V, then it gradually increases and decreases within the range 800 to 700 V. In time 0.6s to 0.8s, the dc-link voltage remains constant and after that a rapid change has occurred which is shown in Fig. 8 (a). The output grid voltage response is shown in Fig. 8 (b). It remains constant in all the time during the variation of the irradiance in PV array. The irradiance has no effect on the output grid voltage waveform. The output grid current response is depicted in Fig. 8 (c). It shows variation in output current for different irradiance condition. When the irradiance is very low, the output current also decreases. The higher irradiance value shows highest amount of output current. The lowest current is 5 A and the highest current is 10 A. The output power response of the grid-tied PV system is demonstrated in Fig. 8(d). The variation of the power response

can be observed from the output power waveform. From 0 to 0.2s, constant output power is observed which is 20 kW. After that, power decreases from 20 to 5 kW in the time period 0.2s to 0.4s and then increases from 5 kW to 20 kW in time period 0.4s to 0.6s. Then the power varied and a rapid change is observed at 0.8s.

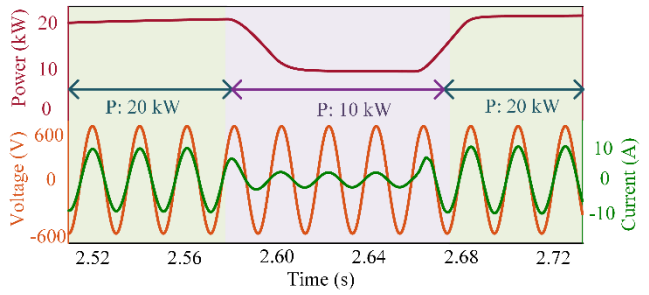

Fig. 9. System behavior for change in active power.

Fig. 9 displays the system behavior of output grid voltage and current with the change in active power reference. The power reference is kept 20 kW in time 2.52 s to 2.58 s, 10 kW in time 2.58 s to 2.66 s and then 20 kW in time 2.66 s to 2.72 s. The output voltage is unaffected during these periods. The grid current changes with the active power reference. This indicates that the proposed controller can handle the instability of the system and back the system to steady-state position.

Sudden load changed response of inverter output current is depicted in Fig 10. The total load of the inverter vary at any time. Sudden load is applied in time 0.6 s to 1.4 s. In this period, the inverter current has increased but shows the sinusoidal nature with the load perturbations. After removing the load, the current tracks the steady-state position within very short time which shows satisfactory dynamic response of the proposed controller.

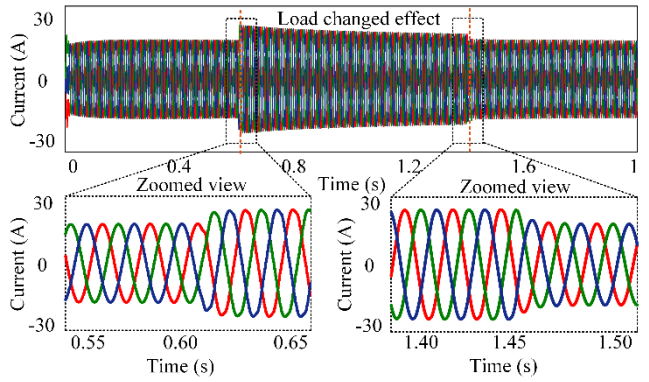

Fig 10. Sudden load changed response of the inverter output current.

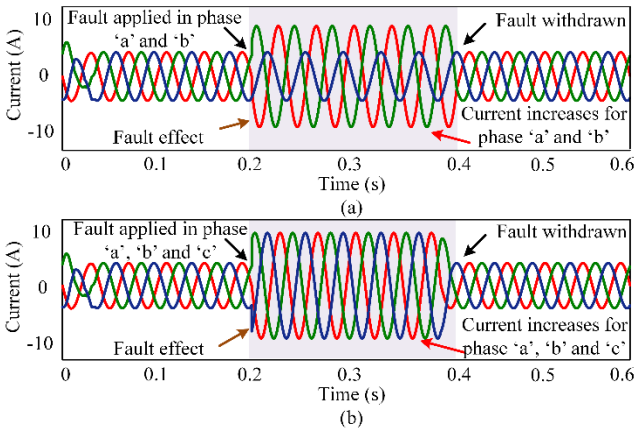

Fig 11. Fault response in output current: (a) fault is applied in phase 'a' and phase 'b'; and (b) fault is applied in phase 'a', phase 'b' and phase 'c'.

Fault effect analysis of grid current under different conditions are observed and depicted in Fig. 11. The fault is inserted in between phase 'a' and phase 'b' which is shown in Fig. 11 (a). In time 0.2 s to 0.4 s, fault is applied to the system. After applying the fault, the currents of phase 'a' and phase 'b' increase and the current of phase 'c' remains constant. After withdrawing the fault, the current of different phases recovers their previous condition. The fault is inserted in between phase 'a', phase 'b' and phase 'c' for time 0.2 s to 0.4 s which is shown in Fig. 11 (b). In this condition, the currents of these three phases increase. This also indicates the fast and robust performance of the system by utilizing the offered control scheme.

The comparative performance of the closed loop system with different controllers are observed to confirm the superiority of the proposed controller. Fig 12 depicts the comparison of dc-link voltages under the load changing period of the system for various control techniques. The dc-link voltage increases when extra load is applied to the system. It shows the response of changing voltage levels according to the controller. In the zoomed view section, voltage level for different controllers are displayed. Propose controller shows the highest voltage of 900 V. The response of changing voltage level during the load change condition for the offered controller is faster than the other controller.

The comparative reference tracking performances in terms of output current waveforms for the proposed controller with PI, PID, PR and PIR controller are shown in Fig. 13. It clearly shows that the proposed controller tracks the reference current efficiently than other controllers. PI and PID controller show higher oscillation in the output current and unable to track the reference. PR and PIR controller also offer some oscillation and provide better response than PI and PID controller. The proposed controller tracts it with almost zero phase difference, less oscillation and distortion which specifies the supremacy of the offered controller.

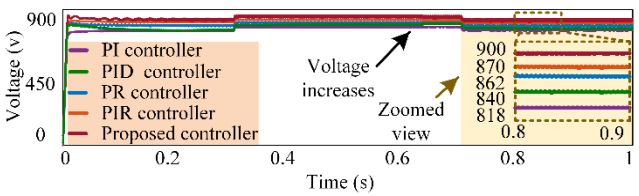

Fig 12. Relative performance of the dc-link voltage of different controllers under the load changing condition.

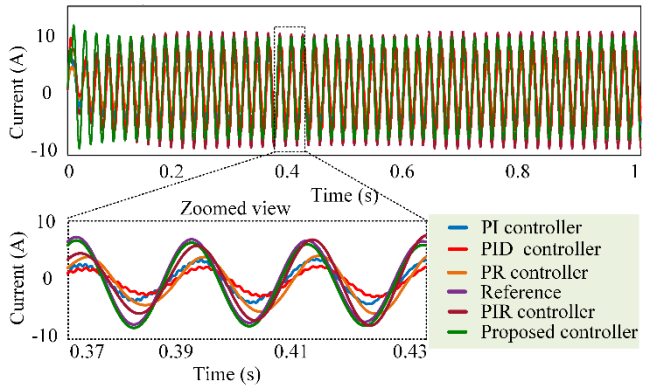

Fig. 13. Comparative performance of reference tracking ability of different controllers.

TABLE I. COMPARATIVE PERFORMANCE ANALYSIS

Controller	dc-link voltage (V)	Grid current (A)	Injected power (kW)	THD of grid current (%)
PI	818	16.31	8.74	20.15
PID	840	15.23	7.92	13.76
PR	862	16.88	8.95	12.21
PIR	870	16.65	8.23	6.76
Proposed PR+LC	900	17.24	9.50	3.33

The comparative performances of the proposed PR+LC controller along with the other controllers including PI, PID, PR and PIR controller are demonstrated in Table I. Table I shows that the proposed controller offers excellent performance than other controllers in terms of dc-link voltage, output grid current, injected power, and THD of grid current. The proposed controller offers higher amount of dc bus voltage, grid current and power comparing with the other control schemes. The grid current THD for the conventional control schemes is higher than 5%. According to IEEE-519 standard, the system will hamper by applying these control techniques to non-isolated inverter-based grid connected system. In contrary, the proposed control scheme offers 3.33% THD which is allowable according to the IEEE standard.

VI. CONCLUSION

In this work, an advanced and fast control technique is proposed for three-phase non-isolated inverter fed grid-connected PV systems. The performance of this offered control scheme is investigated in MATLAB/Simulink environment. Compared with other most popular control methods, this proposed control scheme offers lowest THD for output current and better conversion efficiency for the inverter. The proposed control technique also provides better response in changing level of dc-link voltage and reference tracking ability compared with the conventional PI, PID, PR and PIR controllers. It also delivers convincing performance in dynamic responses for sudden load changed condition and fault handling capability of the grid-connected PV system. Thus, the proposed control technique could be an emerging choice for the expansion of medium voltage grid along with other industrial applications.

REFERENCES

[1] R. Rahimi, M. Farhadi, G. R. Moradi, B. Farhangi and S. Farhangi, " Three-phase filter-clamped transformerless inverter for grid-connected photovoltaic systems with low leakage current,"*IEEE Trans. Ind. Appl.*, doi: 10.1109/TIA.2020.3008134.

[2] K. Niyomsatian, P. Vanassche, J. J. C. Gyselinck and R. V. Sabariego, "Active-damping virtual circuit control for grid-tied converters With differential-mode and common-mode output filters," *IEEE Trans. Power Electron*., vol. 35, no. 7, pp. 7583-7595, July 2020.

[3] B. N. Alajmi, M. I. Marei and I. Abdelsalam, "A multiport DC–DC converterbBased on two-quadrant inverter topology for PV systems," *IEEE Trans. Power Electron*., vol. 36, no. 1, pp. 522-532, Jan. 2021.

[4] S. P. Biswas, M.S. Anower, M.R.I. Sheikh, M. R. Islam, M. A. Rahman, M. A. P. Mahmud, and A. Z. Kouzani, " A modified reference saturated third harmonic injected equal loading PWM for VSC-based renewable energy systems," *IEEE Trans. Appl. Supercond.*, doi: 10.1109/TASC.2021.3096484.

[5] A. M. Mahfuz-Ur-Rahman, M. R. Islam, K. M. Muttaqi and D. Sutanto, "Model predictive control for a new magnetic linked multilevel inverter to integrate solar photovoltaic systems with the power grids," *IEEE Trans. Ind. Appl*., vol. 56, no. 6, pp. 7145-7155, Nov.-Dec. 2020.

[6] R. Rahimi, S. Farhangi, B. Farhangi, G. R. Moradi, E. Afshari and F. Blaabjerg, "H8 inverter to reduce leakage current in transformerless three-phase grid-connected photovoltaic systems," *IEEE J. Emerg. Sel. Topics Power Electron.*, vol. 6, no. 2, pp. 910-918, Jun. 2018.

[7] S. Jahan, S. P. Biswas, M. K. Hosain, M. R. Islam and K. M. Muttaqi, "Performance analysis of current control techniques of modular multilevel converter for grid connected photovoltaic system," In *Proc. 2020 Australasian Universities Power Engineering Conf. (AUPEC)*, Hobart, Australia, 29 Nov.-2 Dec. 2020, pp. 1-6.

[8] Y. Han, H. Chen, Z. Li, P. Yang, L. Xu and J. M. Guerrero, "Stability analysis for the grid-connected single-phase asymmetrical cascaded multilevel inverter with SRF-PI current control under weak grid conditions," *IEEE Trans. Power Electron*., vol. 34, no. 3, pp. 2052-2069, Mar. 2019.

[9] S. Jahan, S. P. Biswas, S. Haq, M. R. Islam, M. A. P. Mahmud and A. Z. Kouzani, "An advanced control scheme for voltage source inverter based grid-tied PV systems," *IEEE Trans. Appl. Supercond*., doi: 10.1109/TASC.2021.3094446.

[10] Y. Jia, J. Zhao and X. Fu, "Direct grid current control of LCL-filtered grid-connected inverter mitigating grid voltage disturbance," *IEEE Trans. Power Electron.*, vol. 29, no. 3, pp. 1532-1541, Mar. 2014

[11] S. Jahan, S. P. Biswas, M. K. Hosain, M. R. Islam, S. Haq, A. Z. Kouzani, and M. A. P. Mahmud, "An advaned control technique for power quality improvement of grid-tied multilevel inverter," *Sustainability*, vol. 13, no. 2, p. 505, Jan. 2021.

[12] M. M. Rahman, S. P. Biswas, M. A. Rahman, M. R. Islam and K. M. Muttaqi, "A second order high performance resonant controller for a three-phase islanded microgrid," In *Proc. 2020 IEEE Industry Applications Society Annual Meeting*, Detroit, MI, USA, 10-16 Oct. 2020, pp. 1-6.